ELSEVIER

image AND vision COMPUTING

Feature-based image registration by means of the CHC evolutionary algorithm[☆]

O. Cordón [a], S. Damas [b,*], J. Santamaría [b]

[a] *Department of Computer Science and A.I. University of Granada, Granada, Spain*
[b] *Department of Software Engineering, University of Granada, Granada, Spain*

Abstract

Image registration has been a very active research area in the computer vision community. In the last few years, there is an increasing interest on the application of evolutionary computation in this field and several evolutionary approaches have been proposed obtaining promising results. In this contribution we introduce the use of an advanced evolutionary algorithm, CHC, to solve the 3D image registration problem. The new proposal will be validated using different shapes (both synthetic and magnetic resonance images, and with several of the latter affected by noise and occlusion), considering four different transformations for each of them, and comparing the results with those from ICP, from the usually applied binary-coded genetic algorithms, and from real-coded genetic algorithms.
© 2006 Elsevier B.V. All rights reserved.

Keywords: Image registration; Genetic algorithms; CHC; Iterative closest point

1. Introduction

Image registration (IR) [4] is a fundamental task in image processing used to finding a correspondence (or transformation) among two or more pictures taken under different conditions: at different times, using different sensors, from different viewpoints, or a combination of them. On the other hand, evolutionary computation (EC) [1] uses computational models of evolutionary processes as key elements in the design and implementation of computer-based problem solving systems. Genetic algorithms (GAs) [18,20] are maybe the most known evolutionary algorithms.

In the last few years, there is an increasing interest on applying EC fundamentals to IR. Unfortunately, we can find a lack of accuracy when facing this problem and different contributions fall into simplifications of the problem or, even worse, do not apply EC concepts in the more suitable way. In this contribution we propose the use of an advanced evolutionary algorithm, CHC [10], to solve the 3D IR problem.

To do so, in Section 2 we give some IR basics. Next, we make a critical review of the different approaches to the IR problem from the perspective of EC in Section 3. Section 4 describes our proposal, which is tested in Section 5 over different images and transformations, considering also a number of noise and occluded instances. Finally, in Section 6 we present some conclusions and new open lines for future works.

2. Image registration

IR can be defined as a mapping between two images (I_1 and I_2) both spatially and with respect to intensity: $I_2(x,y,z,t) = g(I_1(f(x,y,z,t)))$. We can usually find situations where intensity difference is inherent to scene changes, and thus intensity transformation estimation given by g is not necessary. That is the scenario considered by *feature-based registration* methods, which focus their attention on relevant geometric primitives invariant to the f function. That will be the case of the current contribution. Besides, we will consider f represents a *similarity* transformation, i.e. rotation, translation and uniform scaling.

Although the final registration problem solution consists of the right values for the parameters which determine f, two different approaches arise, each of them working in a different solution space: (i) to search for the optimal geometric primitives correspondence in the matching space and then identify the appropriate transformation parameters to overlay the scene and the model images (I_1 and I_2, respectively)

E-mail addresses: ocordon@decsai.ugr.es (O. Cordón), sdamas@ugr.es (S. Damas), jsantam@ugr.es (J. Santamaría).

considering such matching [2,3,7,6,12], and (ii) to directly search in the parameter space, computing the matching between scene and model geometric primitives to validate the estimated transformation once it has been applied, as we shall see in the following section [25]. While the former involves determining which of the scene primitives match each model one, the latter deals with the estimation of the registration transformation causing this model-scene overlapping.

One of the most known feature-based algorithms for IR is the iterative closest point (*ICP*), proposed by Besl and McKay [3] based on the former approach (matching space search), and extended in different papers [26]:

- A point set P is given with N_p points p_i from the data of the scene. The model X is defined by N_x supporting geometric primitives: points, lines, or triangles.
- The iteration is initialized by setting $P_0 = P$, the registration transformation by $q_0 = [1,0,0,0,0,0,0]^t$, and $k = 0$. The next four steps are applied until convergence within a tolerance threshold $\tau > 0$:
1. Compute the matching (Y_k) between the current scene (P_k) and the model points (X) by the closest point assignment rule: $Y_k = C(P_k, X)$
2. Compute the registration transformation: $f_k(P_0, Y_k)$
3. Apply the registration transformation: $P_{k+1} = f_k(P_0)$
4. Terminate iteration when the change in mean square error falls below τ.

The algorithm has important drawbacks [3]: (i) it is sensitive to outlier presence; (ii) the initial states for global matching play a basic role for the method success when dealing with important deformations between model and scene points; (iii) the estimation of the initial states is not a trivial task, and (iv) the cost of a local adjustment can be important if a low percentage of occlusion is present.

Hence, the algorithm performance is not good with important transformations. As stated in [26]: 'we assume the motion between the two frames is small or approximately known'. This is a precondition of the algorithm to get reasonable results.

Besides feature-based IR, there are other approaches to other variants of the IR problem that search for the best f function in the parameter space. A recent and interesting contribution is the one proposed by Chen et al. [5] where the authors analyze a global optimization technique to study the input images returned by two sensors, which cover circular regions such that the two readings overlap. Likewise, in [17] Hill and Taylor describe the application of genetic algorithms in model-based image interpretation. Nevertheless, that is not the assumption of the current contribution since in our approach the registration is performed taking as a base the information derived from the shape.

3. Evolutionary computation and image registration

An exhaustive review of the different approaches to the IR problem from the perspective of EC is out of the scope of our study. Nevertheless, we will mention some of the most important aspects of them in order to achieve a deep understanding of our work. These registration contributions usually solve the problem directly searching in the parameter space instead of searching for the optimal matching in the matching space.

The first attempts to solve IR using EC can be found in the early 1980s. The size of data as well as the number of parameters that are looked for, prevent from an exhaustive search for the solutions. Such an approach based on a GA was proposed in 1984 for the 2D case and applied to angiographic images [13]. Since this initial contribution, different authors solved the problem but we can still find important limitations in their approaches:

- The use of a binary coding to solve an inherent real coding problem, with the precision problem depending on a given number of bits in the encoding [14,25].
- The kind of GA considered, usually Holland's original proposal [18]. This GA was proposed almost 30 years ago and it suffers from several drawbacks later solved by other genetic components and/or more advances evolutionary algorithms. Contributions [14,25][1] follow this approach.
- Many approaches only handle images suffering a translation and a rotation transformation [14,16,25], which is not the case in many real situations where at least the consideration of a uniform scaling is desirable. The resulting similarity transformation suits the registration of aerial and satellite images, bony structures in medical images, and brain multimodal images, among others [15].

The use of the CHC algorithm (to be described in Section 4) is found in [14]. In such a contribution, it is not a new proposal but it is employed to compare the 2D rigid registration results of the authors proposal to those from the CHC algorithm. Nevertheless, as we shall see in Section 5, we will prove how the good treatment of this algorithm allows us to obtain the best results in the current 3D IR problem.

Notice that we are tackling with the specific IR problem where the aim is to obtain the concrete f transformation function achieving the best overlapping between the scene and the model. A similar problem is the object shape alignment in pattern recognition where the goal is to decide whether two dissimilar images are originated from different items, or belonged to the same object but viewed from different camera positions [24]. However, we will not consider the latter approach in the current contribution since it refers to a different problem.

4. A CHC evolutionary algorithm for image registration

Two different evolutionary IR algorithms will be proposed using the original binary CHC algorithm and a real-coded

---

[1] This contribution is slightly improved respect to Holland's proposal as it progressively adjusts the search space and the mutation probability.

version in order to solve the different drawbacks introduced in the previous section. Below, we describe their components.

4.1. The original binary-coded CHC

The key idea of the CHC binary-coded evolutionary algorithm [10] involves the combination of a selection strategy with a very high selective pressure, and several components inducing a strong diversity. The four main components of the algorithm are shown as follows:

- An *elitist selection*. The M members of the current population are merged with the offspring population obtained from it and the best M individuals are selected to compose the new population. In case that a parent and an offspring have the same fitness value, the former is preferred to the latter.
- A *highly disruptive crossover*, HUX, which crosses over exactly half of the non-matching alleles, where the bits to be exchanged are chosen at random without replacement. This way, it guarantees that the two offspring are always at the maximum Hamming distance from their two parents, thus proposing the introduction of a high diversity in the new population and lessening the risk of premature convergence.
- An *incest prevention mechanism*. During the reproduction step, each member of the parent (current) population is randomly chosen without replacement and paired for mating. However, not all these couples are allowed to cross over. Before mating, the Hamming distance between the potential parents is calculated and if half this distance does not exceed a difference threshold d, they are not mated and no offspring coming from them is included in the offspring population. The aforementioned threshold is usually initialized to $L/4$ (with L being the chromosome length). If no offspring is obtained in one generation, the difference threshold is decremented by one.

The effect of this mechanism is that only the more diverse potential parents are mated, but the diversity required by the difference threshold automatically decreases as the population naturally converges.

- A *restart process*, substituting the usual GA mutation, which is only applied when the population has converged. The difference threshold is considered to measure the stagnation of the search, which happens when it has dropped to zero and several generations have been run without introducing any new individual in the population. Then, the population is reinitialized by considering the best individual as the first chromosome of the new population and generating the remaining $M-1$ by randomly flipping a percentage (usually a 35%) of their bits.

4.2. The real-coded CHC extension

We have extended the binary-coded CHC to deal with real-coded chromosomes, maintaining its basis as much as possible.

Real-coded CHC is based on the same four main components than classical binary-coded CHC [11]. The elitist selection and the restart are exactly the same in both cases. However, there is a need to adapt the incest prevention mechanism (whose operation is guided by the Hamming distance) and to work with a different crossover operator (since HUX is specifically designed for binary-coded chromosomes).

In order to be able to measure the similarity between two parents using the Hamming metric, we consider a binary conversion of both of them. The difference threshold d is then proportionally set up imitating the classical CHC. It is initialized to $D_{max}/4$, where $D_{max} = \sum_{i=1}^{N} param_i \cdot nbits_i$ (with N being the number of parameters to be estimated in our IR problem, and $nbits_i$ being the number of bits used to code the ith parameter). So, the crossover is avoided if the distance between both parents is lesser than d. Hence, every time no offspring is included in the population after a generation, the difference threshold d is decremented by one and, as usual, the restart is triggered when $d \leq 0$.

On the other hand, the BLX-α crossover is considered to substitute the HUX one [11]. Hence, the parameter α allows us to make this crossover as disruptive as desired. This crossover operator is based on obtaining one offspring $H = (h_1,...,h_i,...,h_n)$ from two parents $C_1 = (c_1^1, ..., c_n^1)$ and $C_2 = (c_1^2, ..., c_n^2)$ by uniformly generating a random value for each gene h_i in the interval $[c_{min} - I\alpha, c_{max} + I\alpha]$, with $c_{max} = \max(c_i^1, c_i^2)$, $c_{min} = \min(c_i^1, c_i^2)$, and $I = c_{max} - c_{min}$. Two offspring are generated by applying twice the operator on the two parents.

Despite the empirical performance of the binary-coded CHC and the real-coded CHC (to be analyzed in Section 5), note the minimum computational increase of this extension resulting from: (i) a real to binary-coded conversion (in order to compute the Hamming distance), and (ii) instead of crossing over half of the non-matching alleles choosing the bits to be exchanged at random (HUX), now a uniform random value is generated for each gene (BLX-α). As we will show in Section 5, these changes will not have an impact neither in the speed of the algorithm nor in its convergence rate.

4.3. Components of our CHC-based image registration algorithm

4.3.1. Coding scheme

The 3D similarity transformation with uniform scaling factor is determined fixing seven parameters, which will be the ones we will look for. That is: $(\alpha_x, \alpha_y, \alpha_z, \Delta_x, \Delta_y, \Delta_z, S)$, where α_i are the three Euler angles, Δ_i are the three components of the displacement vector and S is the uniform scaling factor. Hence, these seven parameters are binary or real coded in the chromosome depending on the algorithm variant applied.

4.3.2. Fitness function

In this contribution, we propose a fitness function to avoid the influence of outliers and mismatching in the final solution. To do so, we consider the use of a grid data structure in order to improve the efficiency of the closest point assignment

computation [25]. Since we are searching in the parameter space and we work on a discrete grid, when defining our fitness function we must prevent cases where scene points are transformed to spatial locations outside the ranges where the grid is defined [8]. Therefore, in such a situation we must assign a low fitness value.

Otherwise, we will try to estimate the parameters of the transformation, which transform the scene points and lead us to the maximization of function F in

$$F = \left[E(N_{insidegrid}/N_s) \left(1/1 + \sum_{i=0}^{N_s} \|GCP(T(y_i))\|^2 \right) + (N_{insidegrid}/N_s) \right]$$

where, E is the floor function, $N_{insidegrid}$ is the number of scene points inside the grid when the registration transformation T encoded in the chromosome is applied to the scene, N_s is the number of scene points, and $GCP(T(yi))$ is the GCP function [25] (returning the model closest point to every cell center) applied to the result of transforming the y_i scene point.

It can be seen that $F \in [0,2]$, so that an individual with a fitness value lesser than 1 encodes a bad transformation putting some of the points out from the working grid, while those individuals with $F \geq 1$ correspond to transformations being able to keep the set of scene points inside the grid. Hence, the larger the F value, the better (since this means that the distance between the scene and the model set of points is closer to zero).

5. Experiments

We present a number of experiments to study the performance of our proposals. These tests have been carried out under the same conditions since we wanted to extend our conclusions to other possible situations. The results obtained by our two CHC variants, binary *BinCHC* and real-coded *RealCHC*, will be compared against those obtained by *ICP* [26] (see Section 2), by a binary-coded GA[2] (*BinGA*) and by a real-coded GA[3] (*RealGA*). We will also study the behavior of the previously mentioned algorithms in a noisy scenario, where occlusion is present as well.

5.1. Model and scene images

Our results correspond to a number of registration problems with synthetic and 3D medical images. All of them have suffered the same four global similarity transformations, which must be estimated by the different evolutionary algorithms applied. In order to properly evaluate every IR method, these 'ground-truth' transformation are previously known (see Section 5.3).

Vertices defining the 3D mesh related to the first synthetic shape have been chosen as feature points (4623 vertices). We

will refer to this first image as 'Dragon' (upper left image in Fig. 1). The first registration scenario is the easiest one: the scene and the model images are the same (the synthetic 'Dragon' image) and they differ on the four similarity transformations to be estimated.

Because of the amount of data to be managed when tackling real images, it is necessary to develop a preprocessing step in order to extract a set of feature points to describe the surfaces. Feature points are obtained applying a 3D crest lines edge detector [21] to a brain isosurface from a magnetic resonance image (MRI), returning 1052 points. We will refer to it as the 'Brain1' image (upper right image in Fig. 1), which is presented in [23] (a similar one is used in [22], and considered in our previous works [8,6]). The second registration scenario considers the four transformations to be applied to this real MRI, hence the scene and model again only differ on their pose, but now they both are real images.

A similar feature selection process has been carried out in the next two realistic T1 MRIs of a normal brain from the *BrainWeb* database at McGill University [19]. The first one, named as 'Brain2' (bottom left image in Fig. 1) was originally composed of more than thirty thousands data points but subsequently reduced in order to accelerate the algorithmic convergence of every IR method. The resulting MRI scene is comprised by 583 feature points. Besides, in order to test the performance of our proposal when facing difficult noisy and occluded environments, the second MRI (model image) is a different one, named 'Brain3' (bottom right image in Fig. 1). After the aforementioned preprocessing step, 284 feature points have been selected from 'Brain3'. This image inherently presents a multiple sclerosis lesion (see circle in Fig. 1), as well as a 5% of Gaussian noise. The noise percentage is relative to the average real and imaginary values of the overall brightest tissue class and it represents the percent ratio of the standard deviation of the white Gaussian noise versus the signal for a reference tissue [19]. Therefore, the third registration scenario not only considers real MRIs with different geometric orientation, but the scene and the model do not correspond to the same image.

5.2. Parameter settings

All the parameter settings are shown in Table 1. Every method is run for the same fixed time of 20 s on a 2200 MHz. Pentium IV processor. In order to avoid execution dependence, 15 different runs of each algorithm are performed. In the binary-coded evolutionary algorithms (*BinGA* and *BinCHC*), large individuals have been considered as we aim at getting precise solutions for each transformation parameter. This leads us to define our binary chromosome as a 105 bits structure (15 bits for each of the seven parameters). Crossover and mutation probabilities in both *BinGA* and *RealGA* are $P_c = 0.6$ and $P_m = 0.1$, while $\alpha = 0.5$ in *RealGA* and *RealCHC*. Finally, the population size is $M = 100$ individuals in every case.

---

[2] This is the proposal of Yamany et al. [25] using the fitness function described in Section 4.3.2.

[3] This is the proposal of He and Narayana [16] adapted to solve the 3D IR problem.
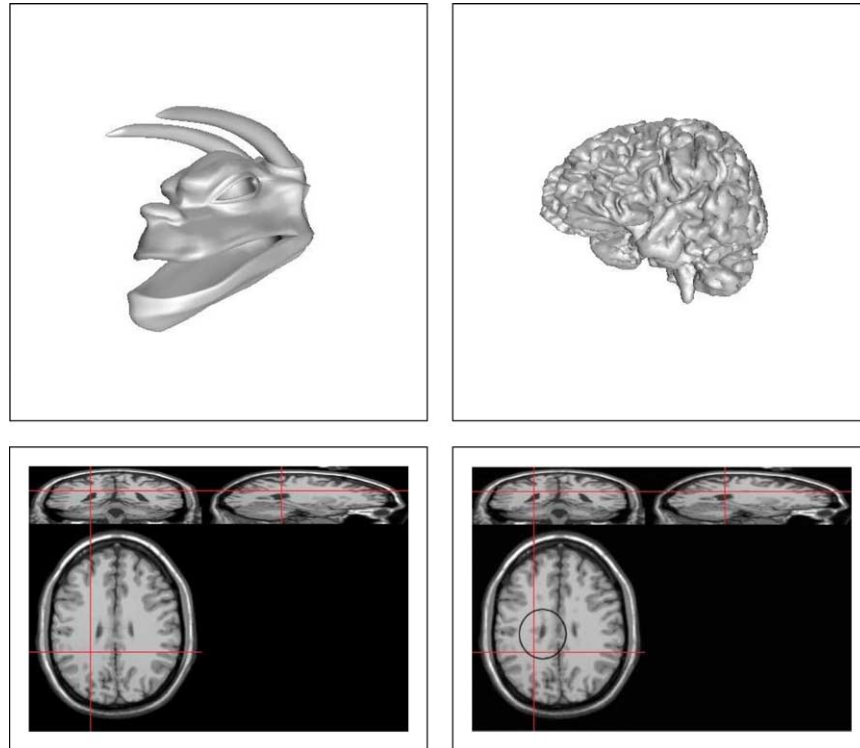
Fig. 1. Input images. The two first problem scenarios (first row, 'Dragon' and 'Brain1' images) consider there is a geometric transformation to be estimated between the scene and the model, both comprised by the same image. Despite the complexity of the previous IR problems, the third scenario considers the same geometric transformations in a noisy environment with the original MRI scene 'Brain2' (bottom left) and the MRI model 'Brain3' (bottom right) including a multiple sclerosis lesion (see circle) and an 5% of Gaussian noise.

5.3. Transformations to be estimated

The four 'ground-truth' transformations considered are stored in Table 2. In such table all the 3D rotations have been expressed in terms of rotation angle ($RAngle°$) and rotation axis ($RAxis_x$, $RAxis_y$, $RAxis_z$) to achieve a better understanding of the geometric transformation involved. If we analyze these parameters, we can see the important transformations to be estimated: both rotation and translation vectors represent a strong change in the object location. In fact, the lowest rotation angle is 95°. Meanwhile, translation values are also high. Likewise the scale factor ranges from 0.7 (in the first transformation) to 2 (in the fourth one). These transformations can be appreciated from the four IR instances of the 'Dragon' image, depicted in Fig. 2, which shows different views of the

initial pose of both the transformed scene, in blue (dark gray), and the model, in yellow (light gray), images.

5.4. Results

Notice that all the statistics in this section are based on a usual error measure in the IR field, the *mean square error* (*MSE*): $MSE = \sum_{i=1}^{N} \|f(x_i) - y_i'\|^2/N$, where, f is the estimated registration function, x_i is a scene point, with y_i' being its closest point in the model, and N is the number of features in the scene.

Tables 3–5 show the performance of the ICP estimation, the classical binary-coded GA, the real-coded GA and the two versions of our CHC-based proposal, respect to the three test IR scenarios. As said, all the statistics presented correspond to fifteen different runs of every evolutionary algorithm and transformation with a different seed. Fig. 3 graphically shows the best absolute estimations (x_{best} values in Table 3) of the

Table 1
Parameter settings of the different algorithims

Common settings	
Population size: 100 individuals	
Run time: 20 s	
Number of runs: 15 runs	
Binary-coded EAs	Real-coded EAs
Genes per chromosome: 105	α value (BLX-α): 0.5
Gas	
Crossover probability: $P_c = 0.6$	
Mutation probability: $P_m = 0.1$	

Table 2
Applied transformations to every 3D image

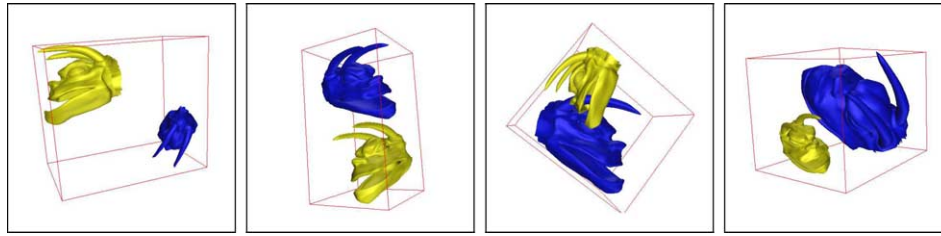|	Tr.1	Tr. 2	Tr.3	Tr.4
Rot angle°	122.699997	95	180.6	202.5
Rot axis$_x$	0.727393	0	−0.11547	−0.536895
Rot axis$_y$	0.363696	1	0.80829	0.59655
Rot axis$_z$	−0.581914	0	−0.57735	0.59655
Δ_x	7.568	−1.5	−7.5	24
Δ_y	−15.97	19.969999	−12	10.6
Δ_z	−23.879999	2.8	10.8	5.2
S	0.7	1	1.5	2

Fig. 2. Different views of the four transformations to be estimated (see Table 2).

'Dragon' image achieved by our real-coded CHC proposal. Meanwhile, Fig. 4 shows the four ICP estimations for the mentioned image. We can see the overlapping of the original and transformed images is almost perfect in every real-coded CHC scenario[4] but in the third transformation (Fig. 3) where neither ICP nor the EAs solve the IR problem properly. All of them get stuck in a local optimum.

Likewise, Fig. 5 shows the best absolute estimations (x_{best} in Table 4) of the 'Brain1' image achieved by our real-coded CHC proposal. Fig. 6 shows the ICP results for the aforementioned image. It depicts that the only acceptable ICP solution is the estimation of the second transformation.

Finally, Fig. 7 shows the best absolute estimations (x_{best} in Table 5) of the *Brain*2 vs. Tr_i(*Brain*3) scenario achieved by our real-coded CHC proposal. Fig. 8 shows the ICP results for the aforementioned scenario. Again, the registrations obtained by the former clearly outperform those from the latter.

We can see that the GAs outperform ICP in seven of the eight noise-free experiments developed. ICP only achieves a good solution for the second transformation applied to the 'Brain1' image (see Table 4). Figs. 4 and 6 show the four ICP estimations for the 'Dragon' and 'Brain1' images, respectively, when they are applied to the original image (in blue -dark gray-). Such results only overlap these images and the transformed ones using the Table 2 parameters (in yellow -light gray-) in the case of the second transformation of the 'Brain1' image (Fig. 6). This behavior would have been desirable if the results had been precise enough. It is specially important to notice the good and stable performance of our real-coded CHC proposal in the noise-free experimentation, with the best mean MSE value in all the eight experiments developed. Besides, the binary-coded CHC still achieves better results than both Yamany et al. binary-coded GA and He and Narayana's real-coded GA in half of the experiments (it outperforms them in every experiment developed in the 'Brain1' image and achieves very similar results in the 'Dragon' image).

Meanwhile, the different tests considering noise and occlusion show again the robustness of our proposal (specially remarkable when compared to ICP). Therefore, it is shown the good behavior of the fitness function proposed in this paper (Section 4.3.2) to face the first drawback of ICP enumerated in

---

[4] If a perfect matching between the original and the transformed image is achieved, the visualization software shows either yellow -light gray- pixels (representing the transformed object) or blue -dark gray- ones (depicting the method's estimation).

Table 3
MSE of the four transformations in Table 2, applied to the 'Dragon' image (statistics from 15 different runs)

Method		Dragon vs Tr_i(Dragon)			
		Tr. 1	Tr. 2	Tr. 3	Tr. 4
ICP		0.7034	1.09	3.21	4.07
Binary-coded EAs					
GA_{bin}	x_{best}	0.3365	0.6689	1.6088	3.0736
	$\bar{x}$	0.3769	**0.7036**	1.6886	3.2204
	σ	0.0362	0.0265	0.0704	0.1507
CHC_{bin}	x_{best}	0.3365	0.6746	1.6687	2.9895
	$\bar{x}$	**0.3613**	0.7257	**1.6762**	**2.9990**
	σ	0.0132	0.0488	0.0059	0.0050
Real-coded EAs					
GA_{real}	x_{best}	0.1612	0.6625	1.5946	2.8362
	$\bar{x}$	0.3385	0.7653	1.6540	3.0786
	σ	0.0968	0.0732	0.0313	0.1779
CHC_{real}	x_{best}	0.0001	0.0000	1.4834	0.0003
	$\bar{x}$	**0.2672**	**0.3973**	**1.6413**	**1.7826**
	σ	0.1344	0.3244	0.0789	1.4553

Best binary and real-coded algorithm estimations are highlighted using bold font.

Table 4
MSE of the four transformations in Table 2, applied to the 'brain1'image (statistics from 15 different runs)

Method		Brain vs Tr_i (Brain 1)			
		Tr. 1	Tr. 2	Tr. 3	Tr. 4
ICP		324.16	0.00	1024.77	931.14
Binary-coded EAs					
GA_{bin}	x_{best}	0.0007	0.0023	0.0301	0.0040
	$\bar{x}$	1.9440	3.7900	2.4979	5.1755
	σ	2.2249	3.2141	30.1295	1.5301
CHC_{bin}	x_{best}	0.0035	0.0029	0.0054	0.0272
	$\bar{x}$	**0.0053**	**0.0450**	**0.2795**	**0.2436**
	σ	0.0017	0.0817	0.2916	0.2019
Real-coded EAs					
GA_{real}	x_{best}	0.1526	0.0609	0.4718	1.2787
	$\bar{x}$	0.2205	0.1059	0.7797	2.0297
	σ	0.0557	0.0273	0.4042	0.6397
CHC_{real}	x_{best}	0.0001	0.0026	0.0039	0.0047
	$\bar{x}$	**0.0034**	**0.0050**	**0.0061**	**0.0444**
	σ	0.0007	0.0006	0.0007	0.0040

Best Binary and real-coded algorithm estimations are highlighted using bold font.

Table 5
MSE of the four transformations in Table 2, applied to the 'Brain 2' to be aligned with 'Brain 3' image (statistics from 15 different runs)

Method		Brain vs Tr_i (Brain 3)			
		Tr.1	Tr.2	Tr.3	Tr.4
ICP		417.66	449.59	2415.25	7115.64
Binary-coded EAs					
GA_{bin}	x_{best}	23.93	48.48	109.21	196.22
	$\bar{x}$	48.18	71.9	**220.24**	446.15
	σ	17.73	28.32	95.75	130.08
CHC_{bin}	x_{best}	23.87	48.38	108.77	194.53
	$\bar{x}$	**31.41**	**60.58**	316.91	**291.15**
	σ	21.37	23.70	304.62	105.34
Real-coded EAs					
GA_{real}	x_{best}	23.86	48.71	112.23	198.76
	$\bar{x}$	24.64	49.44	123.77	220.29
	σ	0.72	0.65	7.97	14.39
CHC_{real}	x_{best}	23.84	48.39	108.50	194.47
	$\bar{x}$	**23.88**	**48.52**	**116.78**	**194.59**
	σ	0.08	0.11	28.85	0.12

Best binary and real-coded algorithm estimations are highlighted using bold fonts.

Fig. 3. *RealCHC* estimations corresponding to the four transformations considered for the 'Dragon' image.
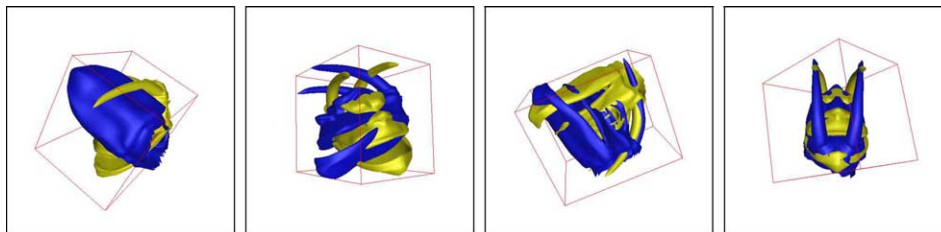

Fig. 4. *ICP* estimations corresponding to the four transformations considered for the 'Dragon' image.

Section 2. That is, the influence of outlier presence in the final solution. Real-coded CHC achieves the best mean estimations in all the four noisy IR tests. Moreover, the lowest standard deviation values related to real-coded CHC show the robustness of the algorithm.

As we mentioned in Section 4.2, despite the overall better empirical performance of the real-coded CHC, there are no hidden costs associated to this extension. On the one hand, for each generation, a real to binary number conversion must be performed for every chromosome in the real-coded CHC
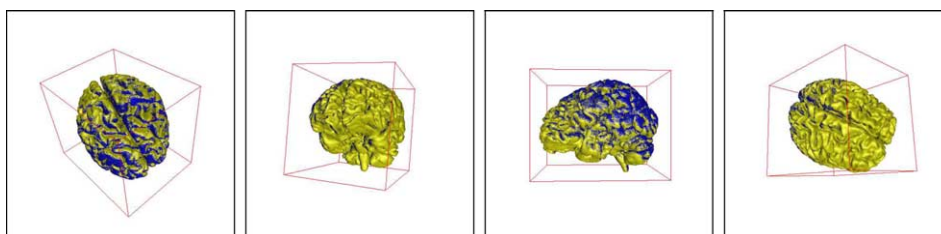

Fig. 5. *RealCHC* estimations corresponding to the four transformations considered for the 'Brain1' image.
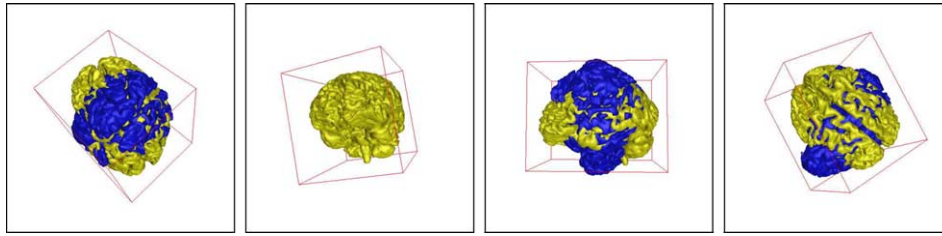
Fig. 6. *ICP* estimations corresponding to the four transformations considered for the 'Brain1' image.
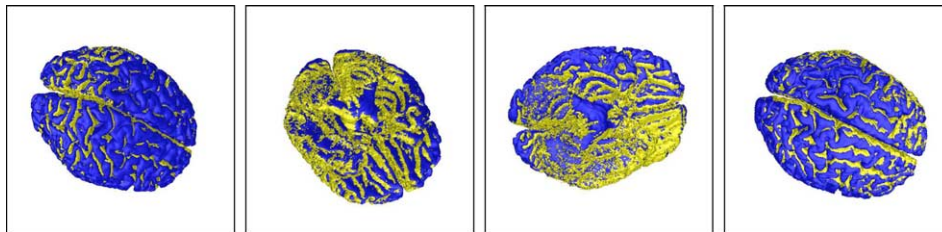

Fig. 7. *RealCHC* estimations corresponding to the four transformations considered for the $Brain2$ vs. $Tr_i(Brain3)$ scenario.
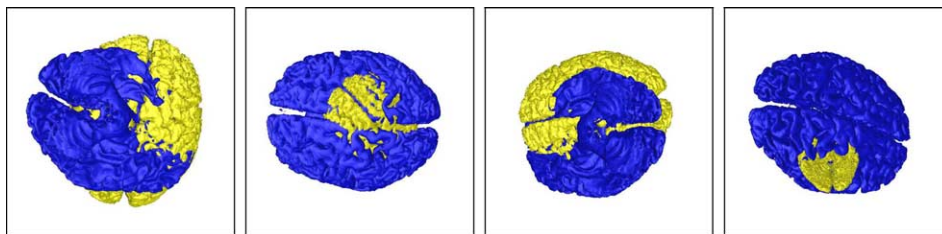

Fig. 8. *ICP* estimations corresponding to the four transformations considered for the $Brain2$ vs. $Tr_i(Brain3)$ scenario.

population. Nevertheless, such conversion allows a faster convergence to solutions of better quality, since the algorithm reaches more promising areas in the search space. This behavior is shown in Fig. 9, with the MSE averaged convergence curve of the fifteen runs of every evolutionary algorithm when solving one of the four most complicated IR instances, i.e. $Brain2$ vs. $Tr_4(Brain3)$.
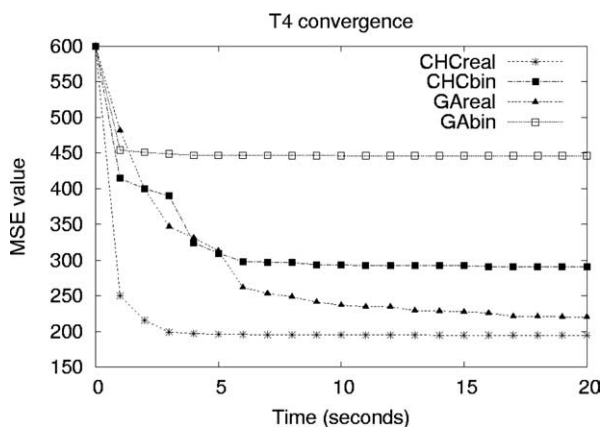

Fig. 9. Averaged convergence curves of the 15 runs of every EA when tackling the $Brain2$ vs. $Tr_4(Brain3)$ IR problem.

6. Concluding remarks and future works

In this contribution, we have faced the feature-based 3D IR problem using an advanced evolutionary algorithm, CHC. First, we have presented different drawbacks of previous evolutionary approaches to the problem. In order to avoid these restrictions, we have proposed two different IR algorithms from the original CHC considering a new fitness function, which allows us to avoid the negative effect of bad matching due to the presence of noise and occlusion in the images. A number of experiments have been applied to validate our contribution. To do so, different previous proposals of feature-based IR algorithms have been considered as baselines: ICP [3] (one of the most known feature-based IR algorithms), as well as two state of the art evolutionary proposals [16,25]. Three different IR scenarios and four different similarity transformations for each of them have been considered, resulting in a total number of twelve IR problems (eight without noise and another four affected by noise and occlusion). It has been shown how CHC solutions outperform those obtained by the other approaches when considering both noisy and noise-free scenarios.

There is a number of new open lines to be done after this proposal: there is a need to develop a deep study of the

behavior of different EC-based algorithms when dealing with the IR problem. Moreover, new advanced diversity induction mechanisms should be tested in order to study their performance in that problem.

References

[1] T. Bäck, D.B. Fogel, Z. Michalewicz (Eds.), Handbook of Evolutionary Computation, IOP Publishing Ltd, Bristol, 1997.

[2] E. Bardinet, S. Fernández-Vidal, S. Damas, G. Malandain, N. Pérez de la Blanca, Structural object matching, in: Second International Symposium on Advanced Concepts for Intelligent Vision Systems (ACIVS 2000), vol. II, Baden-Baden, Germany, 2000, pp. 73–77.

[3] P.J. Besl, N.D. McKay, A method for registration of 3-D shapes, IEEE Transactions on Pattern Analysis and Machine Intelligence 14 (1992) 239–256.

[4] L.G. Brown, A survey of image registration techniques, ACM Computing Surveys 24 (4) (1992) 325–376.

[5] Y. Chen, R.R. Brooks, S.S. Iyengar, N.S.V. Rao, J. Barhen, Efficient global optimization for image registration, IEEE Transactions on Knowledge and Data Engineering 14 (2002) 79–92.

[6] O. Cordón, S. Damas, Image registration with iterated local search, Journal of Heuristics 12 (1-2) (2006) 73–94.

[7] O. Cordón, S. Damas, E. Bardinet, 2D Image registration with iterated local search in: J.M. Benítez, O. Cordón, F. Hoffmann, R. Roy (Eds.), Advances Soft Computing-Engineering Design and Manufacturing, Springer, Berlin, 2003, pp. 233–242.

[8] O. Cordón, S. Damas, J. Santamaría, A CHC evolutionary algorithm for 3D image registration, in: Lecture Notes in Artificial Intelligence, vol. 2715, Heidelberg, Springer, Berlin, 2003, pp. 404–411. Proceedings of the 10th International Fuzzy Systems Association World Congress (IFSA'03). Istanbul, Turkey.

[10] L.J. Eshelman, The CHC adaptive search algorithm: how to safe search when engaging in non traditional genetic recombination, in: G.J.E. Rawlins (Ed.), Foundations of Genetic Algorithms, Morgan Kaufmann, San Mateo, 1991, pp. 265–283.

[11] L.J. Eshelman, Real-coded genetic algorithms and interval schemata, in: L.D. Whitley (Ed.), Foundations of Genetic Algorithms 2, Morgan Kaufmann, San Mateo, 1993, pp. 187–202.

[12] S. Fernández-Vidal, E. Bardinet, S. Damas, G. Malandain, N. Pérez de la Blanca, Object representation and comparison inferred from its medial axis, in: International Conference on Pattern Recognition (ICPR 00), vol. 1, Barcelona, Spain, 2000, pp. 712–715.

[13] J.M. Fitzpatrick, J.J. Grefenstette, D. Van Gucht, Image registration by genetic search, in: IEEE Southeast Conference, Louisville, USA, 1984, pp. 460–464.

[14] G. Garai, B.B. Chaudhuri, A cascaded genetic algorithm for efficient optimization and pattern matching, Image and Vision Computing 20 (4) (2002) 265–277.

[15] A.A. Goshtasby, Z- and 3-D Image Registration for Medical, Remote Sensing, and Industrial Applications, Wiley, New York,NY, 2005.

[16] R. He, P.A. Narayana, Global optimization of mutual information: application to three-dimensional retrospective registration of magnetic resonance images, Computerized Medical Imaging and Graphics 26 (2002) 277–292.

[17] A. Hill, C.J. Taylor, Model-based image interpretation using genetic algorithms, Image and Vision Computing 10 (5) (1992) 295–300.

[18] J.H. Holland, Adaptation in Natural and Artificial Systems, The University of Michigan Press, Ann arbor, 1975 (The MIT Press, London, 1992).

[19] R.K.S. Kwan, A.C. Evans, G.B. Pike, MRI simulation-based evaluation of image-processing and classification methods, IEEE Transactions on Medical Imaging 18:11 (1999) 1085–1097.

[20] Z. Michalewicz, Genetic Algorithms + Data Structures = Evolution Programs, Springer, Berlin, 1996.

[21] O. Monga, R. Deriche, G. Malandain, J.P. Cocquerez, Recursive filtering and edge tracking: two primary tools for 3D edge detection, Image and Vision Computing 9 (4) (1991) 203–214.

[22] X. Pennec, N. Ayache, J.P. Thirion, Landmark-based image registration using features identified through differential geometry, in: I. Bankman (Ed.), Handbook of Medical Imaging, Academic Press, New York, 2000, pp. 499–513. (Chapter 31).

[23] J.P. Thirion, A. Gourdon, Computing the differential characteristics of isointensity surfaces, Computer Vision and Image Understanding 61 (2) (1995) 190–202.

[24] P.W.M. Tsang, A genetic algorithm for aligning object shapes, Image and Vision Computing 15 (11) (1997) 819–831.

[25] S.M. Yamany, M.N. Ahmed, A.A. Farag, A new genetic-based technique for matching 3D curves and surfaces, Pattern Recognition 32 (1999) 1817–1820.

[26] Z. Zhang, Iterative point matching for registration of free-form curves and surfaces, International Journal of Computer Vision 13 (2) (1994) 119–152.